Resolution of the threshold fracture energy paradox for solid particle erosion

Peck, Daniel Thomas; Volkov, Grigory; Mishuris, Gennady; Petrov, Yuri

Published in:
Philosophical Magazine

DOI:
10.1080/14786435.2016.1240378

Publication date:
2016

Citation for published version (APA):
Peck, D. T., Volkov, G., Mishuris, G., & Petrov, Y. (2016). Resolution of the threshold fracture energy paradox for solid particle erosion. *Philosophical Magazine*. https://doi.org/10.1080/14786435.2016.1240378

Resolution of the threshold fracture energy paradox for solid particle erosion

Daniel Peck[a,d], Grigory Volkov[b,c], Gennady Mishuris[a*], Yuri Petrov[b,c]

[a] *Aberystwyth University, Penglais, Aberystwyth, UK, SY23 2BZ;*
[b] *St.Petersburg State University, Universitetsky Pr-t., 27, 198504 Petergof, St.Petersburg, Russia;*
[c] *Institute of problems of mechanical engineering RAS, Bolshoy Pr-t V.O., 61, 199178 St.Petersburg, Russia;*
[d] *ISOTOP Ltd., Canot Industry Zone, 20 Hayarok st., Gedera, 7075001, Israel.*

(*Received 00 Month 20XX; accepted 00 Month 20XX*)

Previous models of a single erosion impact, for rigid axisymmetric indenter defined by shape function $z = B^{1-\lambda} r^{\lambda}$, have shown that a critical shape parameter $\lambda^* = 5.5$ exists which determines the behaviour of the threshold fracture energy. However repeated investigations into this parameter have found no physical explanation for its value. Again utilizing the notion of incubation time prior to fracture, this paper attempts to provide a physical explanation of this phenomena by introducing a supersonic stage into the model. The final scheme allows for the effect of waves along the indenters contact area to be taken into account. The effect of this physical characteristic of the impact on the threshold fracture energy and critical shape parameter λ^* are investigated and discussed.

Keywords: Erosion; Fracture; Incubation time; Supersonic; Blunt impact; Elastic half-space;

1. Introduction

Erosion impacts are a widely studied phenomena, the understanding of which has yielded valuable insights into the physical mechanisms at play, which has in turn allowed for the improvement of technologies which either rely on preventing erosion based damage or utilizing the resulting energies. The study of erosion induced fracture, particularly for small indenter sizes, has however often been seen as at best a secondary concern, despite certain technologies being notably susceptible (e.g. parametric resonance screens [1]). Additionally, conventional models often only examine prescribed indenter shapes, potentially meaning that important effects may be overlooked.

The need for differing models for small sized indenters became apparent during experimental research examining erosion fracture, through studies into the threshold velocities of impacting particles [2, 3]. These investigations revealed an interesting phenomenon, namely that values of the threshold velocity for particles with a relatively large radius are approximately the same, whereas reducing the radius leads

*Corresponding author. Email: ggm@aber.ac.uk

to a significant increase in the threshold velocities. It was concluded that, as the impact duration primarily depends on the particle size, the set of threshold velocity values have to be divided into two branches: one static, for large-size particles, and the other dynamic, for small-sized indenters. However the conventional approach when studying the strength problem only permits one to calculate values of the threshold velocities by applying the critical stress criterion, and as such can only explain the static branch [4].

A more effective analytical model, capable of explaining the nature of origin for both the static and dynamic branches, was developed in [5]. The initial model provided the solution of the contact problem for a spherical particle impacting an elastic half-space, with the approach later being generalized for particles of different shapes [6, 7]. These approaches looked at the problem of erosion induced fracture from an energy costs point of view. In particular they examined the threshold fracture energy, which is the kinetic energy required to induce erosion based fracture. This was made possible by utilizing an incubation time based fracture criterion to estimate the parameters of the tensile stress pulses which characterize erosion fracture.

As these models developed however, it soon became clear that there was an unexplained phenomena at play. In [6], which utilized the Hertz solutions for erosion impact, it was observed that there existed a minimum threshold fracture energy in the case of a spherical, but not cylindrical, indenter. The subsequent investigation [7], which utilized the Shtaerman-Kilchevsky theory of quasi-static blunt impact for an indenter whose arbitrary shape function: $z = B^{1-\lambda} r^{\lambda}$ describes a set of smooth paraboloids, observed that there existed a critical shape parameter $\lambda^* = 5.5$, with indenters characterized by $\lambda < \lambda^*$ having a unique minimum threshold fracture energy, while no such minimum existed when $\lambda > \lambda^*$. However neither paper was able to provide a physical explanation for this critical value. A later paper attempted to unearth clues by improving on the accuracy of the previous approach, achieved by examining fixed spacial points for which the stress function was maximized [8], however this was similarly unsuccessful in explaining the value of the critical shape parameter.

While these previous models successfully incorporated various dynamic aspects into the modeling, notable dynamic effects where ignored. For example, the existence of a supersonic stage, where the speed of the contact zone boundary exceeds the elastic wave propagation velocity in the condensed matter, was shown in [9, 10]. Borodich adduced the proof of this statement for the convex contact surfaces based on geometrical principles in [11]. It is noteworthy that only the quasi-static approaches of Hertz and Shtaerman for the contact problem were used during the previous analysis.

In this paper we attempt to show that the mystery surrounding this parameter was due to a failure of previous approaches to take into account the dynamic properties of the elastic medium. Towards this end, we will examine the threshold fracture energy, as well as the critical shape parameter λ^*, in more detail by incorporating supersonic modeling of the initial stages of the impact. We consider the supersonic stage in a similar way to that applied by Argatov for a spherical indenter in [12]. Utilizing the general solution proposed by Borodich [11] we create a model for which the maximal impact stress and threshold fracture energy are more sensitive to the physical characteristics of the impact. This will notably ensure that the impact characteristics take account of the wave velocity within the impacted medium. The choice of Borodich's solution is stipulated by the fact that it describes only the supersonic stage and is based on the common principles which have historically

been used by other researchers [9, 10, 13–15]. It should be also noted that both theories neglect the effect of friction at the contact interface, which does play a role, especially for oblique impacts [16]. This simplifying assumption is often made in the literature [17] in the case of normal impact incidence, and as this paper is primarily aiming to examine the viability and effects of such an approach only the simplest form of each regime will be examined.

The paper is organized as follows. Sect. 2 sees the construction of the model for a single erosion impact during the various regimes. In Sect. 2.1 *Borodich's* solution for the supersonic stage is stated, and the resulting set of equations determining the initial moments of the impact are formulated. Following this in Sect. 2.2 the relevant equations from the previous model by *Argatov et al* are given, with some being rederived to account for the new initial conditions when entering the subsonic stage. Finally in Sect. 2.3 any discontinuities between the two approaches are eliminated. The numerical results are detailed in Sect. 3. We briefly introduce the incubation time based fracture criterion in Sect. 3.1, before formulating the initial algorithm and calculating the threshold fracture energy for various λ in Sect. 3.2, with some details being relegated to Appendix. A. This is followed by an examination and discussion of the critical shape parameter in Sect. 3.3. Finally the important results are collated and discussed in Sect. 4.

2. Construction of approximate solution for the penetration process

2.1. *Supersonic stage. Borodich's solution*

The general solution of the contact problem during the supersonic stage was presented by Borodich [11], and allows one to obtain the temporal dependencies of both the contact force and the penetration depth. General formulas for an arbitrary convex shaped indenter were presented, with specific shapes in the form of a cone, elliptic paraboloid and a pyramid being evaluated. We use the results from [11] to find the mechanical parameters of the process in the supersonic regime for a axisymmetric blunt indenter, defined by the shape function:

$$z = B^{1-\lambda} r^{\lambda}, \tag{1}$$

where $\lambda > 1$ and B is a constant having dimension $[length]$. Then the value $S(w)$ of contact area is related to the penetration depth w as:

$$S(w) = \pi B^{2-\frac{2}{\lambda}} w^{\frac{2}{\lambda}}. \tag{2}$$

In an accordance with Borodich solution, the time dependence for the penetration depth w can be implicitly calculated as follows:

$$\begin{gathered} t(W) = \int_0^W \frac{dw}{V_0 - \frac{\rho c \pi}{m\mu} B^{3-\mu} w^{\mu}}, \\ \mu = \frac{\lambda + 2}{\lambda}, \quad 1 < \mu < 3, \end{gathered} \tag{3}$$

where V_0 and m are initial velocity and mass of the projectile respectively, ρ is elastic media density and c is the velocity of the longitudinal waves. Some simple

algebraic transformations of (3) yield:

$$\begin{aligned} t(W) &= \frac{w_s}{V_0}\int_0^{\frac{W}{w_s}} \frac{d\xi}{1-\xi^\mu}, \\ w_s &= B\left(\frac{\mu m V_0}{\pi\rho c}B^{-3}\right)^{\frac{1}{\mu}} \end{aligned} \tag{4}$$

Thus we know the function $F(y,\mu)$, which implicitly describes the relationship between the penetration depth w and the time t

$$F(y,\mu) = \int_0^y \frac{d\xi}{1-\xi^\mu}, 0 < y < 1 \tag{5}$$

It should be noted that $F(y,\mu)$ is a monotonic increasing function over $0 < y < 1$ for every $1 < \mu < 3$, and its value increases from zero to infinity. It is however possible to determine the inverse function, F^{-1}, which allows us to obtain the particular solution for a considered projectile shape.

As a result, the supersonic indentation of a blunt indenter into the elastic half-plane is defined by the following relationship (5):

$$w_d(t) = w_s F^{-1}\left(\frac{V_0}{w_s}t\right), \tag{6}$$

while the other problem parameters: the indenter velocity, $V_d(t)$, and total force, $P_d(t)$, are given by the following relations:

$$\begin{aligned} V_d(t) &= \dot{w}_d(t) \\ P_d(t) &= \pi\rho c V_d(t) B^2 \left(\frac{w_d(t)}{B}\right)^{\mu-1} \end{aligned} \tag{7}$$

The end of the supersonic stage, denoted t_*, is that moment in time when the outward velocity of the contact area becomes equal to velocity of the longitudinal waves c. The value of t_* can be calculated as the solution to the equation

$$\dot{a}(t_*) = c, \tag{8}$$

where the longitudinal wave speed is that of a one-dimensional solid, namely:

$$c = \sqrt{\frac{E}{\rho}}$$

equation (8) can be written in the form:

$$\dot{a}(t_*) = \frac{1}{\lambda}\left(w_d(t_*)\right)^{\frac{1}{\lambda}-1} B^{\frac{\lambda-1}{\lambda}} V_0 \left(1 - \left(\frac{w_d(t_*)}{w_s}\right)^\mu\right) \tag{9}$$

Thus, one can now evaluate the time t_* and calculate boundary values of the penetration depth $w_* = w_d(t_*)$, contact radius, $a_* = a_d(t_*)$, and the projectile velocity $V_* = V_d(t_*)$.

Moreover, one can observe that $t_* \to 0$ as $\rho \to 0$.

Unfortunately there are no exact solutions for the stress distribution during the supersonic stage, only the normal stresses for the central point $r = 0$ of projectile

2.2. *Subsonic stage. Shtaerman-Kilchevsky theory*

During the subsonic stage ($t > t_*$) we utilize the Shtaerman-Kilchevsky theory, which has previously been applied to the case of quasi-static blunt impact by Argatov, Mishuris, Petrov [7]. The relationship between the contact force $P_{qs}(t)$ and penetration depth $w_{qs}(t)$ can be written as:

$$P_{qs}(t) = k_1 w_{qs}^{\frac{\lambda+1}{\lambda}} \tag{10}$$

where

$$k_1 = \frac{E}{1-\nu^2} B^{\frac{\lambda-1}{\lambda}} \frac{2^{\frac{2}{\lambda}} \lambda^{\frac{\lambda-1}{\lambda}}}{\lambda+1} \Gamma\left(\frac{\lambda}{2}\right)^{-\frac{2}{\lambda}} \Gamma(\lambda)^{\frac{1}{\lambda}} \tag{11}$$

here E and ν are the Young modulus and Poisson ratio for the elastic media, $\Gamma(x)$ is a Gamma function. The equation of motion for a projectile with mass m can be written as follows:

$$\begin{gathered} m\frac{d^2 w_{qs}}{dt^2} = -k_1 w_{qs}^{\beta}, \\ \beta = \frac{\lambda+1}{\lambda} \end{gathered} \tag{12}$$

The solution obtained for the supersonic stage gives following initial conditions [7]:

$$w_{qs}(t_*) = w_*, \quad \frac{dw_{qs}}{dt}|_{t=t_*} = V_* \tag{13}$$

Multiplying both sides of equation (12) by $\frac{dw}{dt}$ before integrating, we obtain:

$$\frac{m}{2}(V_{qs}^2 - {V_*}^2) = -\frac{k_1}{\beta+1}(w_{qs}^{\beta+1} - {w_*}^{\beta+1}) \tag{14}$$

The maximum penetration depth w_0 can be calculated by substituting $V_{qs} = 0$ into equation (14)

$$w_0 = \left(\frac{(\beta+1)m{V_*}^2}{2k_1} + {w_*}^{\beta+1}\right)^{\frac{1}{\beta+1}} \tag{15}$$

A second integration of (14) gives us the the temporal dependence of the penetration depth $w_{qs}(t)$ during the subsonic stage

$$\int_{t_*}^{t} dt = t - t_* = \Delta t = w_0 \sqrt{\frac{m(\beta+1)}{2k_1 {w_0}^{\beta+1}}}\, U\big(\frac{w_{qs}}{w_0}, \beta\big) \tag{16}$$

where

$$U(\frac{w_{qs}}{w_0},\beta)=\int_{\frac{w_*}{w_0}}^{\frac{w_{qs}}{w_0}}\frac{dh}{\sqrt{1-h^{\beta+1}}} \tag{17}$$

Thus, the estimated time, t_{qs}, when the penetration reaches its maximum value w_0 is as follows

$$\int_{t_*}^{t_0}dt=t_0-t_*=t_{qs}=w_0\left(\frac{m(\beta+1)}{2k_1{w_0}^{\beta+1}}\right)^{\frac{1}{2}}U(1,\beta) \tag{18}$$

where t_0 is time duration of the load stage. Using (15) this can transformed into:

$$t_0=t_*+\frac{w_0}{V_*}\sqrt{1-\frac{2k_1w_*^{\beta+1}}{(\beta+1)\,mV_*^2+2k_1w_*^{\beta+1}}}\,U\left(1,\beta\right) \tag{19}$$

Since damping occurs, due to the quasi static nature of the formulation, the duration of the unload stage $t_{**}-t_0$ exaggerates the value t_0. For this reason we have to solve the equation (12) one more time with the new initial conditions:

$$w_{qs}(t_0)=w_0,\qquad \frac{dw_{qs}}{dt}\big|_{t=t_0}=0 \tag{20}$$

The first integration give us the projectile velocity in the reverse direction:

$$\frac{dw_{qs}}{dt}=-\sqrt{\frac{2k_1{w_0}^{\beta+1}}{(\beta+1)m}}\cdot\sqrt{1-\left(\frac{w_{qs}}{w_0}\right)^{\beta+1}}. \tag{21}$$

Thus, the value of t_{**} can be determine from the following expression:

$$t_{**}-t_0=w_0\sqrt{\frac{(\beta+1)m}{2k_1{w_0}^{\beta+1}}}\int_0^1\frac{dh}{\sqrt{1-h^{\beta+1}}} \tag{22}$$

Note that $t_{**}-t_0>t_0$. Indeed, the latter is equivalent to

$$w_0\sqrt{\frac{(\beta+1)m}{2k_1{w_0}^{\beta+1}}}\int_0^{\frac{w_*}{w_0}}\frac{dh}{\sqrt{1-h^{\beta+1}}}>t_*,$$

2.3. *Coupling of the solutions for supersonic and subsonic stages*

Because of the peculiarities of the dynamic solution by Borodrich and quasi-static solution by Shtaerman, the function which describes the temporal dependence of the contact area radius will be discontinuous at the time t_*. This is due to the fact that the supersonic and subsonic stages have different physical principles determining the relationship between penetration depth and contact area, and the penetration depth $w(t)$ is continuous in this model (by design). In order to avoid this irregularity, let us

introduce the smooth function $\chi(x)$, which continuously matches the two solutions within the interval $[0.95t_*, 1.05t_*]$

$$\chi(t) \quad = \quad \begin{cases} 1, & 0 < t < 0.95t_* \\ 0, & 1.05t_* < t \end{cases}. \tag{23}$$

Also, we employ this function $\chi(x)$ to sew the contact force $P(t)$, the equation of which also has a discontinuity at the point t_*.

$$\begin{aligned} a(t) &= a_d(t)\chi(t) + a_{qs}(t)\big(\chi(t) - 1\big), \quad 0 < t < t_{**} \\ P(t) &= P_d(t)\chi(t) + P_{qs}(t)\big(\chi(t) - 1\big), \quad 0 < t < t_{**}. \end{aligned} \tag{24}$$

Additionally the mean contact area, which allows us to calculate the stress field under the projectile, is defined as $p_0 = P/(\pi a^2)$ and can be approximated in a similar way:

$$p_0(t) = \frac{P_d(t)}{\pi a_d^2(t)}\chi(t) + \frac{P_{qs}(t)}{\pi a_{qs}^2(t)}\big(\chi(t) - 1\big), \quad 0 < t < t_{**}. \tag{25}$$

Since Borodich's solution does not contain any information about the surface stresses, we enrich the quasi-static solution by extrapolating the corresponding results into the supersonic stage. Thus, the distribution of the contact pressure beneath an indenter with the considered shape is given by

$$\sigma_z(r,t) \equiv p(r,t) = \frac{\lambda + 1}{2} p_0(t) \int_0^{\sqrt{1-r_0^2}} \left(r_0^2 + \xi^2\right)^{\frac{\lambda-2}{2}} d\xi. \tag{26}$$

where $r_0 = r_0(r,t) = r/a(t)$ is the dimensionless radial coordinate. Similarly the radial stress will be approximated by

$$\sigma_r(r,t) \quad = \quad \begin{cases} -p(r_0) + \dfrac{1-2\nu}{{r_0}^2} \displaystyle\int_0^{r_0} \eta p(\eta) d\eta, & r_0 \le 1, \\ \dfrac{1-2\nu}{{r_0}^2} \displaystyle\int_0^{1} \eta p(\eta) d\eta, & r_0 > 1. \end{cases} \tag{27}$$

The maximum radial stresses are achieved at the edge of the contact area, where $r_0 = 1$

$$\sigma_r(1,t) = (1-2\nu) \int_0^1 \eta p(\eta) d\eta = \frac{(1-2\nu)\, P}{2\pi a^2}. \tag{28}$$

As a result, at any time during the penetration process, the approximated solution to the problem will be given by the formulas (25),(26),(28). Note that all of these representations are exact near the ends of the time interval. Indeed, for very small times, Borodich's formulas give the exact solution for the supersonic regime, while the Shtaerman solution precisely describes the projectile behavior during the quasi-static stage.

3. Estimation of the energy costs for the fracture initiation

3.1. *Incubation time fracture criterion*

The previous analysis [7] allows us to produce a lower bound on the fracture pulse of the tensile stresses. Additionally, in [8], it was shown that instead considering the stress pulses for fixed points on the material surface doesn't qualitatively alter the final behavior of the threshold energy in relation to the impact duration. Hence, in the present paper, we employ the lower estimate of the fracture pulses with a view to avoiding additional computational difficulties.

The threshold amplitudes of pulses caused by particle impacts are evaluated using an incubation time approach, which can be effectively applied to explain a number of general dynamic fracture effects caused both by high strain rate and short pulse loading [5, 18, 19]. The corresponding fracture criterion, employed to determine the threshold pulse parameters, is referred to as the incubation time based fracture criterion. In its simplest form, for a brittle fracture, this criterion can be written as follows:

$$\frac{1}{\tau}\int_{t-\tau}^{t}\sigma(\acute{t})d\acute{t} \leq \sigma_c, \tag{29}$$

where σ_c is the static strength of the material and τ is the incubation time of the fracture. This criterion has been successfully used to model a multitude of fracture problems, and has proved itself to be a quite simple and effective method of fracture prediction. It permits us to determine the necessary conditions required for fracture over a wide range of impacts.

3.2. *Estimation of the energy costs for the fracture initiation*

3.2.1. Description of the algorithm

The algorithm used to calculate the threshold fracture energy for a fixed value of λ utilizes the fact that the stress function at the fracture front is a positively valued function, which monotonically increases with increasing v_0. As such we define the following function:

$$\Upsilon\left(v_0\right) = \frac{1}{\tau\sigma_c}\max_{t\in[0,t_{**}]}\left(\int_{t-\tau}^{t}\sigma(\acute{t})d\acute{t}\right) - 1 \tag{30}$$

which has the property that:

$$\Upsilon(v_0)\begin{cases} > 0, & v_0 = v_0^* + \delta \\ \equiv 0, & v_0 = v_0^* \\ < 0, & v_0 = v_0^* - \delta \end{cases} \tag{31}$$

For any arbitrary $\delta > 0$. As such a simple iterative procedure can be utilized in order to obtain v_0^* to a desired level of accuracy.

A second concern is to ensue consistency of results between this paper and the previous investigation [7]. In order to achieve this the constants B and m will have

to be chosen in such a way as to coincide as $\rho \to 0$. This is completed in the first step of the algorithm, and as such the first step could be discarded when carrying out a more general investigation.

With this in place, the algorithm is defined as follows:

(1) Choose an arbitrary t_p, which will approximate t_0. From this calculate the constants B and m using equations (50) and (57) in [7]. Additionally compute an initial expected value of the initial velocity required for fracture initiation, v_p, using equation (56) in the aforementioned paper.

Note: While the value $t_p \to t_0$ as $\rho \to 0$, the two will not be related in this formulation. It is simply an arbitrary starting point chosen to ensure the results are consistent with previous investigations, and is discarded after this step.

(2) Using the value v_p create an initial interval in which v_0^*, the initial velocity required for fracture initiation, is expected to occur (e.g. $v_\delta = [v_p - \delta, v_p, v_p + \delta]$).
(3) Compute the system of equations given in Sect. 2 for each value of v_δ, and obtain the time dependent stress function.
(4) Compute the function $\Upsilon(v_0)$ from (30) for each value of v_δ. Use its properties (31) to obtain a refined interval v_δ containing v_0^*.
(5) Iterate steps 2-4 until a desired level of accuracy is reached. The threshold fracture energy ϵ_0 is then calculated from the obtained v_0^*.

3.2.2. Results for fixed λ

The material constants used in calculations are those for gabbro-diabase [20], which is the same as used in previous investigations of this phenomena [7, 8]. The values are as follows: $E = 6.2 \times 10^9$ N/m^2, $\nu = 0.26$, $\sigma_c = 44.04 \times 10^6$ N/m^2, $\tau = 44$ μs, while the density of the indenter is given by: $\rho_1 = 2400$ kg/m^3. Results are displayed in Fig. 1, for $\lambda = \{2, 3, 4, 5\}$.

It is clear from these results that the threshold fracture energy decreases as the material density ρ increases, however the effect is only apparent for impacts with short durations. This makes intuitive sense, given that v_0 decreases monotonically as the impact duration is increased, and as such the supersonic stage will play a far greater role in rapid impacts.

Additionally, it is immediately apparent from the results in Fig. 1 that the critical shape parameter λ^* will decrease when eroding a more dense material. Furthermore, given that the threshold fracture energy seems to tend to zero for all λ in these graphs, it is safe to assume that the critical shape parameter will have $\lambda^* \to 1$ rapidly as the material density is increased.

3.3. *Critical shape parameter λ^* for various material densities*

3.3.1. Obtaining the critical shape parameter

In previous investigations [7, 8] it was shown that there existed a critical shape parameter, λ^*, with values $\lambda < \lambda^*$ exhibiting a unique non-zero threshold fracture energy (the initial energy required for fracture initiation), while no such minimum existed for $\lambda > \lambda^*$. These studies however assumed a zero-valued density of the

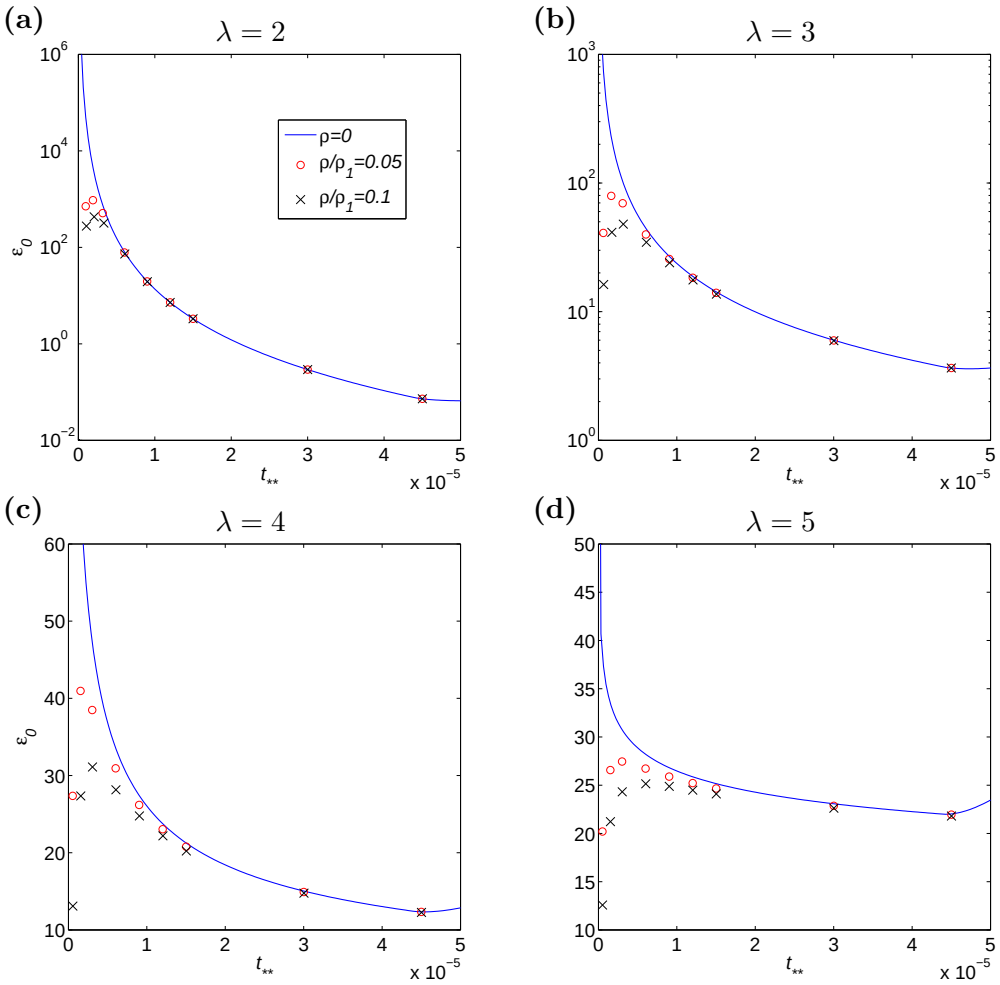

Figure 1. Values of the threshold fracture energy ϵ_0, for various fixed impacted material densities ρ, when (a) $\lambda = 2$ (b) $\lambda = 3$ (c) $\lambda = 4$ (d) $\lambda = 5$. Here $\rho_1 = 2400$ kg/m^3 is the density of the indenter.

impacted medium, and could give no physical explanation for the obtained value $\lambda^* = 5.5$. Here we will attempt to expand on this work, by examining whether the critical shape parameter varies with the density of the impacted material, and as such a physical explanation of the phenomena can be postulated.

The method of obtaining the critical shape parameter λ^* relies on noting the behaviour of the threshold fracture energy for very small impact durations t_{**}. As demonstrated in Fig. 2, when $\lambda < \lambda^*$, the derivative of the threshold fracture energy ϵ_0 will be negative, while this derivative will be positive for $\lambda > \lambda^*$ and zero for the critical shape parameter. As such the algorithm is designed to obtain the sign of this derivative near the origin for a range of λ, before using the results to iteratively work towards the desired critical shape parameter. A full explanation of the algorithm is given below.

(1) Choose a value of the impacted material density ρ. Alongside this an initial overestimate $\lambda_p = [\lambda_1, \ldots, \lambda_n]$ for the potential range of λ^* is taken.
(2) Then, for each $\lambda \in \lambda_p$:

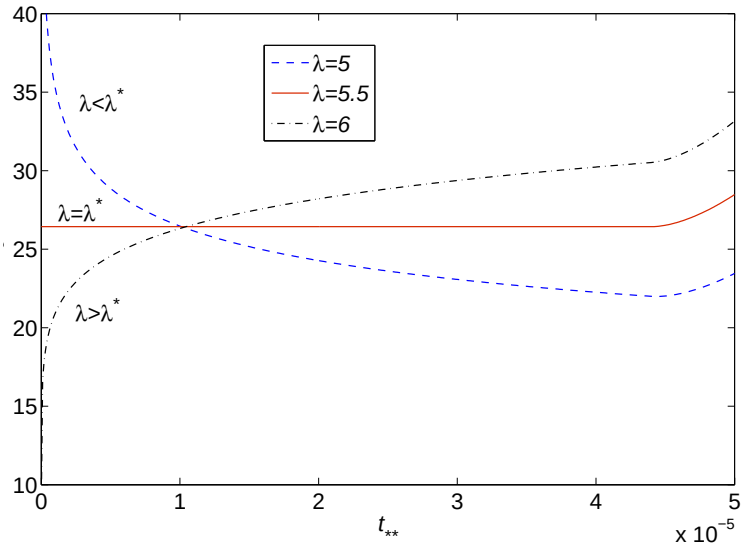

Figure 2. Behaviour of the threshold fracture energy ϵ_0 for small t_{**}, shown here for $\rho = 0$.

- Arbitrary initial points $0 < t_p^1 < t_p^2$ are taken[1]. These approximate t_0 as in the previous algorithm, and must be sufficiently small to predict the behaviour of the derivative of ϵ_0 as $t_{**} \to 0$.
- The threshold fracture energy, ϵ_0, is obtained, for each value of $t_p = \{t_p^1, t_p^2\}$, using the algorithm outlined in Sect. 3.2.1, to a required level of accuracy.
- The derivative of ϵ_0, with respect to t_{**}, is approximated between t_p^1 and t_p^2.

(3) With the value of the derivative obtained for each $\lambda \in \lambda_p$, a new interval in which λ^* exists for the given ρ is obtained.
(4) A new λ_p is defined using the obtained interval for λ_*, and steps 2-3 are repeated until a desired level of accuracy is reached.

This algorithm allows one to obtain the value of λ^* for a given material density ρ, and as such by repeating the we can begin to study the relationship between the impacted material density and the threshold fracture energy. In practice we have found that it is often simpler to instead begin with a value λ, and then iterate to discover the density ρ^* for which it is the critical shape parameter.

3.3.2. Results for various impacted material densities

Numerical simulations were conducted using the same values for the impact parameters as in Sect. 3.2.2, with the addition of taking $t_p = \{2, 2.5\} \times 10^{-6}$ seconds. The results obtained are shown in Fig. 3.

It is clear from this that the critical shape parameter λ^* decreases when impacting materials with higher densities. There is however a clear divergence from previous results which must be expanded upon, which isn't made obvious in the above figure.

[1]Here the values t_p^1, t_p^2 must be small enough to accurately model the asymptotic behaviour, but also not so small as to require infeasible velocities. See Appendix A for a more thorough examination of this choice.

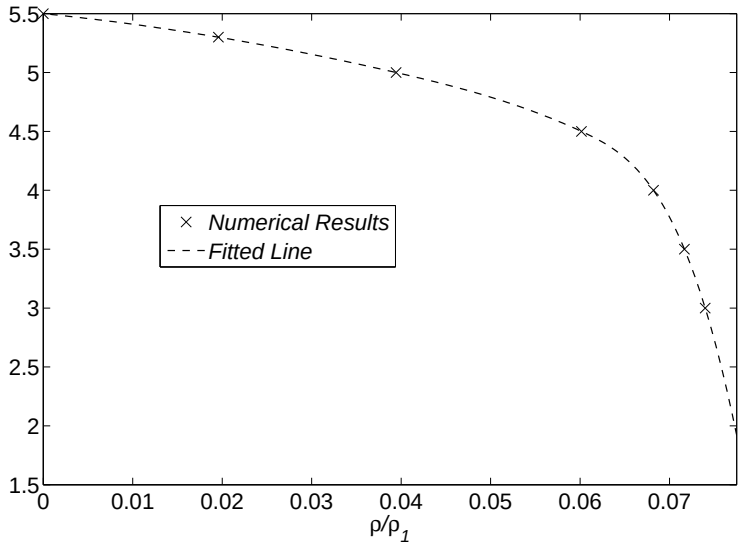

Figure 3. Numerically obtained lower bound of the critical shape parameter λ^* for various impacted material densities ρ. Here $\rho_1 = 2400$ kg/m^3 is the density of the indenter material.

In previous investigations, it has been the case that taking $\lambda = \lambda^*$ will yield a non-unique minimum energy required for fracture. However this will not always be the case under the revised scheme. In order to explain this further, we define the following:

$$\rho^*(\lambda) = \{\rho : \lambda^*(\rho) = \lambda\}$$

An example of the threshold fracture energy, evaluated taking $\rho = \rho^*$ when $\lambda = 3$ is given in Fig. 4.

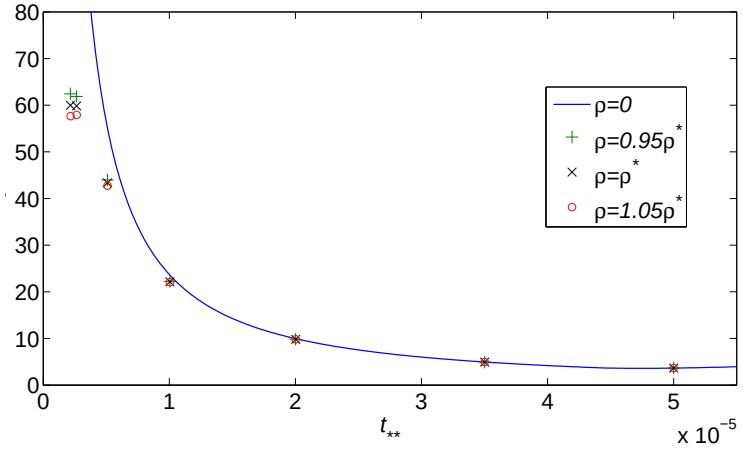

Figure 4. Value of the threshold fracture energy ϵ_0, evaluated when $\lambda = 3$ for $\rho = 0$ (blue line), $\rho = \rho^*$ (black crosses) and $\rho = \rho^* \times 1 \pm 0.05$ (green crosses, red circles). It is clear that a unique minimum occurs for both $\rho \leq \rho^*$, however we will have $\epsilon_0 \to 0$ for $\rho > \rho^*$.

It is clear from this that the minimum energy required for fracture is not unique, however as any increase in the impacted material density results in having $\epsilon_0 \to 0$ as

$t_{**} \to 0$ it is the highest value of λ for which a minimum threshold fracture energy exists. As a result, while this value of λ^* still maintains its most important quality, that of defining the point when a change in case between having a unique threshold fracture energy and none existing occurs, it is of a weaker form than described in previous papers.

4. Discussion and Conclusions

An approach for calculating the threshold fracture energy during erosion impacts with supersonic stages has been derived, and algorithms for obtaining numerical results have been implemented.

The results indicate that the critical shape parameter, λ^*, above which no minimum energy for fracture initiation exists, decreases rapidly as the density of the impacted material increases. This provides evidence to support the proposal that the critical value of the shape parameter $\lambda^* = 5.5$ only emerged in previous modeling due to the fact that the models were only based on the quasi-static approach to contact problem. These results resolve the unanswered questions from previous investigation into this phenomena, showing the dynamic nature of this parameter, and that the value of λ^* depends on the supersonic stage duration determined by the geometry of the contact surfaces and the density of media.

It should be noted that there are possible variations to the approach suggested in this paper, namely as a result of the hypotheses used when gluing together the dynamic and static stages of the contact problem. However there is every reason to believe that they are not meaningful and that the main result would be the same. Also the provided reasoning shows that considering the case of a spherical shaped indenter is more convenient and is naturally supported when constructing such models. The smooth shape of the contact surfaces allows one to avoid irregularities in the solution and unnatural behavior of the process characteristics.

Acknowledgement

DP was supported by the FP7 PEOPLE Marie Curie action project PARM-2 under number FP7-PEOPLE-2012-IAPP while GV, GM and YuP thank for suport to the FP7 PEOPLE Marie Curie IRSES project TAMER under number IRSES-GA-2013-610547. Also GV and YuP are supported by RFBR (14-01-00814, 16-51-53077, 16-01-00638), by the Presidium of the RAS, and Saint Petersburg State University (grant 6.38.243.2014).

References

[1] L. Slepyan and V. Slepyan, J. Phys.: Conf. Ser. 451 (2013) p. 12.
[2] N. Kazarinov, A. Evstifeev, Y. Petrov and V. Lashkov, Doklady Physics 61 (5) (2016) p. 232.
[3] G. Tilly, Wear 23 (1973) p. 87.
[4] C.M. Preece, *Treatise on Materials Science and Technology: Erosion*, Vol. 16, Academic Press, New York, 1979.
[5] Y. Petrov and V. Smirnov, Technical Physics 55 (2) (2010) p. 230.
[6] G. Volkov, N. Gorbushin and Y. Petrov, Mechanics of Solids 47 (5) (2012) p. 491.

[7] I. Argatov, G. Mishuris and Y. Petrov, Philosophical Magazine 93 (19) (2013) p. 2485.
[8] D. Peck, M. Wrobel, G. Mishuris and Y. Petrov, Meccanica 50 (2015) p. 2995.
[9] I. Simonov, Inzh. Zh. Mekhanika Tverdogo Tela 2 (1967) p. 163, (in Russian).
[10] J. Thompson and A. Robinson, Journal of Applied Mechanics 44 (1977) p. 583.
[11] F. Borodich, International Journal of Solids and Structures 37 (2000) p. 3345.
[12] I. Argatov, International Journal of Solids and Structures 45 (2008) p. 5035.
[13] R. Skalak and D. Feit, Trans. A.S.M.E.J. Eng. for Industry B88 (1966) p. 325.
[14] R. Beddings and J. Willis, J. Elast. 6 (1976) p. 195.
[15] A. Gorshkov and D. Tarlakovsky, *Dynamic contact problems with moving boundary*, Nauka, Moscow, 1995, (in Russian).
[16] I. Argatov, N. Dmitriev, Y. Petrov and V. Smirnov, Journal of Friction and Wear 30 (3) (2009) p. 176.
[17] J. Jaeger, Appl. Mech. Rev. 47 (2) (1994) p. 35.
[18] Y. Petrov and A. Utkin, Soviet Materials Science 25 (2) (1989) p. 153.
[19] A. Berezkin, S. Krivosheev, Y. Petrov and A. Utkin, Doklady Physics 45 (11) (2000) p. 617.
[20] Y. Petrov, V. Bratov, G. Volkov and E. Dolmatov, *Incubation time based fracture mechanics and optimization of energy input in the fracture process of rocks*, in *Advances in rock dynamics and applications*, Y. Zhou and J. Zhao, eds., CRC Press, Boca Raton, 2011, p. 163.

Appendix A. Appropriate time intervals

In Sect. 3.3.1 we evaluate the system over some small time interval $t_p = \left\{t_p^1, t_p^2\right\}$, using the results in order to approximate the behaviour of the threshold fracture energy as $t \to 0$. It is clear however that the choice of t_p will influence the final result, and as such we use this appendix to provide further information about how this interval is chosen.

The first problem we examine is that, in the limit, we have that $v_0 \to \infty$ as $t \to 0$. As a result taking points in time too close to zero may lead to results with little applicability to real world situations. In order to investigate further we define:

$$T_{**}(\lambda) = \left\{\max\left(t_{**}\right) : v_0(\lambda, t_{**}) \geq 3 \times 10^8\right\} \tag{A1}$$

which, in other words, provides the smallest impact duration for which the initial velocity is less than the speed of light. This function can be easily obtained by iterative methods, the results of which are shown in Fig. A1.

It is obvious that we must take $t_p^1 > T_{**}(\lambda)$ when conducting any serious investigation, however even taking t_p^1 close to $T_{**}(\lambda)$ will clearly still produce results which rely on infeasible physical characteristics. It is similarly apparent that, as this papers approach relies on the existence of an initial supersonic stage, the initial velocity of the indenter must be sufficiently large for this stage to exist. These constraints place bounds on the values of $t_p^{1,2}$ which can be used, but won't provide an exact interval over which the most representative results may be obtained.

A secondary, although not insignificant, problem facing such an investigation is that of ensuring accurate numerical results. This is particularly apparent for small impact durations, where the extreme values taken by the functions, with

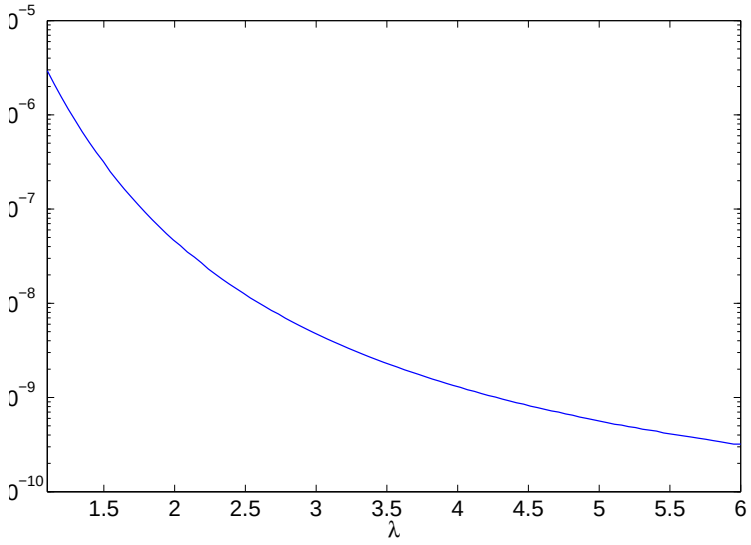

Figure A1. The function (A1) over a range of λ. This curve provides the minimum time duration over which results have any real-world applicability.

the some tending to infinity while others tend to zero, inevitably resulting in a loss of accuracy, particularly during the supersonic stage. This provides not just an additional reason for accepting a lower bound on the value of t_p^1, but also an additional constraint which should be applied to t_p^2. Namely, in order to ensure that inaccuracies in the numerical results don't adversely effect our estimation of the gradient, we must have that the interval t_p is sufficiently large to ensure a significant difference in the values of the threshold fracture energy at either end of the interval. This will decrease the tightness of the lower bound obtained on the value of λ^*, but must be done to ensure reliable results.

Combining the above with the results of numerical experiments it was found that, when maintaining t_p^1 as a constant rather than as a function of λ, the best balance between accuracy and ensuring physically meaningful results was obtained when taking $t_p^1 \approx 2 \times 10^{-6}$, $t_p^2 \approx 2.5 \times 10^{-6}$ seconds.